LA-UR-15-23919 (Accepted Manuscript)

Improved electron collisional line broadening for low-temperature ions and neutrals in plasma modeling

Johns, Heather Marie
Kilcrease, David Parker
Colgan, James Patrick
Judge, Elizabeth
Barefield, James E.
Clegg, Samuel M.

To be published in: Journal of Physics B-Atomic Molecular and Optical Physics ; Vol.48, iss.22, spec. iss.SI, p.224009, Nov 28 2015

DOI to publisher's version: 10.1088/0953-4075/48/22/224009

Permalink to record: http://permalink.lanl.gov/object/view?what=info:lanl-repo/lareport/LA-UR-15-23919

Improved electron collisional line broadening for low-temperature ions and neutrals in plasma modeling

H M Johns[1], D P Kilcrease[1], J Colgan[1], E J Judge[1], J Barefield II[1], R C Wiens[1], and S M Clegg[1]

[1]Los Alamos National Laboratory, Los Alamos NM, 87545, USA

Email: hjohns@lanl.gov

Abstract

Electron collisional broadening of observed spectral lines depends on plasma electron temperature and density. Including this effect in models of measured spectra is necessary to determine plasma conditions; however, computational limits make accurate line broadening treatments difficult to implement in large-scale plasma modeling efforts. In this paper, we report on improvements to the treatment of electron collisional line broadening and illustrate this with calculations using the Los Alamos ATOMIC code. We implement the Dimitrijevic and Konjevic modified semi-empirical model (1986 *Astronomy and Astrophysics* **163** 297 and 1987 *Astronomy and Astrophysics* **172** 345), which we amend by employing oscillator strengths from Hartree-Fock calculations. This line broadening model applies to near-neutral plasmas with electron temperatures of T_e~1eV and electron densities of N_e~10^{17}cm^{-3}. We evaluate the D.K.-inspired model against the previous hydrogenic approach in ATOMIC through comparison to NIST-rated measurements for selected neutral and singly-ionized Ca, O, Fe, and Sn lines using both fine-structure and configuration-averaged oscillator strengths. The new D.K.-inspired model is significantly more accurate than the previous hydrogenic model and we find the use of configuration-averaged oscillator strengths a good approximation for applications such as LIBS (laser induced breakdown spectroscopy), for which we demonstrate the use of the D.K.-inspired model.

PACS: 31.15.A-, 32.20.-r, 32.60.+i, 52.20.Fs

Submit to: Journal of Physics B: Atomic, Molecular, and Optical Physics

1. Introduction

Electron collisional line broadening imparted by the Stark effect on atomic spectral lines from bound-bound transitions in plasmas has been studied for over 50 years. Early work by Baranger derived quantum mechanical [1] and semi-classical [2] approximations for the influence of charged particle collisions on a line using perturbation theory. Electron collisional line broadening is proportional to the density and velocity of the perturber; the latter evolves through approximation into an inverse electron temperature dependence [1-3]. This means overestimating the amount of broadening for a line results in a model that may underestimate the true electron density, or overestimate its temperature. Because each line is broadened to a different extent by electron collisions, an imprecise determination of Stark broadening can result in a model with greater uncertainty in its prediction of line intensity trends for an experimental system. To avoid this situation it is important to include accurate Stark effect broadening for any plasma in which electron collisions are important. We note plasma ions may also impart line broadening through the Stark effect, but as this work considers only electron collisions, our use of the term Stark broadening refers only to electron collisional line broadening.

Modern approaches to Stark broadening calculations include methods such as quantum statistics [4] and close coupling [5] that can be highly accurate for models dealing with isolated lines or sparse spectra. For plasma modeling involving rich spectra containing transition arrays, blended lines, and many-line systems in general, for which computational constraints are a concern, semi-classical models of electron collisional broadening continue to play a vital role [6, 7]. Semi-empirical and semi-classical models simplify calculations by treating electrons as particles traveling a classical path influenced by a dipole interaction between the electron and the ion or neutral atom [3,8-11]. It has been shown that semi-classical approximations can produce results that are very similar to the true quantum mechanical picture if the plasma in question obeys the validity criterion for the approximations behind these modeling efforts [3, 8, 12]. In semi-empirical models, the Gaunt factor applies curvature corrections through a formula designed to mimic a series of experiments or a more complete theory, which is then applied to other cases [8-11, 13-16].

The ATOMIC code [17] has been shown to be capable of modeling such detailed spectra from complex atomic systems. ATOMIC is a plasma spectroscopic modeling code that draws input from the Los Alamos suite of atomic structure and collision codes. These codes supply data such as energy levels, oscillator strengths, and rate coefficients and cross sections for radiative and collisional excitation and ionization processes. ATOMIC uses these atomic structure data and internal equation of state and plasma physics models to output the average ionization stage, plasma emissivity, and opacity as functions of wavelength or photon energy for a given electron temperature and density.

We have recently begun using ATOMIC to model laser-induced breakdown spectroscopy (LIBS) plasmas [17-18]. LIBS plasmas [19] are low temperature ($T_e \sim 1$eV), moderate electron number density ($N_e \sim 10^{17}$cm^{-3}), and mass density ($\rho \sim 10^{-5}$ g/cm^3) systems of neutral and singly ionized atomic species (and sometimes molecules). According to the McWhirter criterion, these systems are typically in LTE for $N_e > 2\text{x}10^{15}$cm^{-3} because electron collisional processes dominate [17, 18]. Experimental data from LIBS systems include moderate resolution portable spectrometers (resolving power ~ 1000) such as the ChemCam instrument on the Mars Science Laboratory [19, 20] and higher resolution 'table-top' systems (>10,000 resolving power) [17]. LIBS plasmas involving geologic samples are complex multi-element systems providing plentiful line rich spectra, and as such present a very useful benchmark for ATOMIC's ability to model plasmas in this regime.

To improve the ability of ATOMIC to model data from moderate resolution spectrometers, the implementation of accurate line broadening models can be important to correctly determine experimental plasma conditions such as T_e and N_e. While ATOMIC includes natural broadening, Doppler broadening, and van der Waals broadening of neutrals, the initial approach to electron collisional broadening has

utilized a hydrogenic approximation [21]. We neglect line broadening caused by the ion microfield because preliminary calculations using an independent model including this effect [22-23] indicate that in the regime we consider, the ion microfield plays a minor role in relation to electron collisional broadening.

The new electron collisional broadening model required for ATOMIC must be computationally fast and should be validated against experimental data. The first stage of this improvement involves the use of the Dimitrijevic and Konjevic modified semi-empirical model from the 1980s [10, 11, 14, 15], which is well known in the astrophysical community. We start by supplementing this model with modern Hartree-Fock atomic structure data calculated by the Los Alamos suite of atomic structure codes. We evaluate the resulting model against NIST critically reviewed and rated measurements of FWHM imparted by electron collisional line broadening for neutral and singly ionized Ca, O, Fe, and Sn [24 -30]. We do not obtain complete agreement with experiment, but utilize this comparison to determine the range of applicability of the new model, and to locate and constrain regions of inaccuracy both for our own work and for researchers elsewhere who utilize similar semi-classical models. We also characterize the relationship between the prior hydrogenic model and the new approach for the benefit of researchers that have relied on the hydrogenic method thus far. In other words, we use validation against experiment to establish a baseline for the new model and to identify and justify a path forward for future work. Although the examples discussed here involve calculations made using ATOMIC, these improvements to electron broadening may be applied to many plasma modeling efforts.

In section 2 we will describe ATOMIC's previous hydrogenic approximation and the new models for electron collisional line broadening of neutrals and ions. In section 3, we discuss the NIST rating systems for measurements of electron collision broadened line shapes and the critical review publications. We will discuss a series of tables for Ca, O, Fe, and Sn in which we compare the results of the new and old model to determine the level of observed improvement and understand continuing differences when compared to experiment. We describe T_e and N_e trends for an example transition, the 4705Å line arising from O II, for the old and new model. In section 4 we demonstrate applications of this model to the analysis of selected lines from LIBS (laser induced breakdown spectroscopy) data. We examine the ChemCam standard for basalt BIR-1A from pre-flight calibrations, an aluminum alloy spectrum, and an iron oxide plasma shot in argon.

2. Electron Collisional Line Broadening Theory

The electron collisional line broadening treatment that has been used in ATOMIC thus far was developed as a high temperature approximation which assumes a large number of scattering channels are accessible and uses the quantum defect hydrogenic matrix element approximation [21]. The line half width half maximum (HWHM) produced by Stark broadening, in energy units, is described below:

$$\hbar\omega = \hbar 8\left(\frac{\pi}{3}\right)^{3/2}\frac{\hbar a_o N_e}{m_e}\sqrt{\frac{E_H}{T_e}}\left\{R_i^2 + R_f^2\right\}, \qquad (1)$$

$$R_j^2 = \frac{1}{2}\frac{E_H}{E_{b,j}}\left\{5n_j^2 + 1 - 3l_j\left(l_j+1\right)\right\}. \qquad (2)$$

For an emission line, the state i refers to an upper level, and the state f to a lower level. The meaning of these subscripts is reversed for absorption lines, but the calculation itself is unchanged. The hydrogenic radial matrix element for the complete set of states interacting with some state j, that could be either i or f, is expressed in equation (2). $E_{b,j}$ is the binding energy of the state j, and E_H is the binding energy for the hydrogen atom. In equation (1) we have a linear dependence on electron number density N_e and an inverse square root dependence on electron temperature T_e. The Bohr radius a_o, mass of the electron m_e, and Planck's constant $\hbar$ are in cgs units, as is N_e. ATOMIC uses eV for both the line width (HWHM) and the temperature so $\hbar$ and E_H are in eVsec and eV respectively.

For near-neutral plasmas existing at low temperatures (<1 to a few eV), this hydrogenic approximation consistently overestimates the amount of electron collision broadening that occurs. In equation (1) each scattering state contributes fully to the broadening. In reality, the amount of broadening imparted by an electron from a given scattering state is based on how energetically accessible it is, but the hydrogenic model does not take this into account because this approximation always selects a Gaunt factor of one.

In order to improve our treatment of near-neutral plasmas, it is desirable to use a model that incorporates electronic structure and treats the amount of broadening provided by each state independently, relative to the energy available from a given perturber and the correction of the Gaunt factor, but has a low computational cost. As a first step, we select the models proposed by Dimitrijevic and Konjevic [10, 11, 14, 15] that have performed well in comparisons to experiment in the literature. In the original papers, the electron collisional broadening of neutrals [14] is expressed in equation (3).

$$\hbar\omega = \hbar\pi\sqrt{\frac{32}{27}}N_e\frac{\hbar a_o}{m_e}\sqrt{\frac{E_H}{T_e}}\left[\sum_{i'}R_{ii'}^2 f_\omega\left(\frac{\Delta E_{ii'}}{3T_e}R_{ii'}\right)+\sum_{f'}R_{ff'}^2 f_\omega\left(\frac{\Delta E_{ff'}}{3T_e}R_{ff'}\right)\right]. \quad (3)$$

$$R_{jj'}^2 = \frac{S_{jj'}}{w_j} = \frac{3E_H}{\Delta E_{jj'}}\frac{w_j f_{jj'}}{w_j}. \quad (4)$$

The semi-empirical neutral Gaunt factor is expressed as the function f_ω, which depends on the ratio between the electron temperature and the energy of the perturbation, as well as the radial matrix element $R_{jj'}$. The simplified approach in [14] utilized hydrogenic radial matrix elements based on the derivation in [10]. Among the atomic structure information used in ATOMIC are the weighted oscillator strengths $w_j f_{jj'}$ calculated by the LANL atomic structure code CATS [31]. While we utilize the fine-structure oscillator strengths for spectroscopic modeling of low temperature plasmas, we save computational time on line broadening by utilizing the configuration-averaged oscillator strength here. As discussed in Cowan's book [31], the radial matrix element squared is the line strength $S_{jj'}$ divided by the statistical weight w_j. This can be related to oscillator strength in equation (4) as a function of the ratio between the binding energy of hydrogen E_H and the transition energy $\Delta E_{jj'} = \left|E_j - E_{j'}\right|$, where the states j and j' again refer to either the initial state i and perturbing state i' or the final state f and its perturbing state f'. While we utilize oscillator strengths in ATOMIC, any accurate calculation of squared radial matrix elements or line strengths could also be used. We make no changes to the f_ω function from [14]. The derivation for this function and the simplified line width expression in equation (3) is described in [10,14], based on the method of Griem [8, 9].

For ions, rather than use the simplified version of the Dimitrijevic and Konjevic model [15] we rely on the original and more complete derivation [11] based on the semi-empirical model derived in [3, 8, 9]. In equation (5) we utilize the line width formula from [11]. As with the neutral model, we utilize the weighted oscillator strengths already present in ATOMIC to obtain the radial matrix elements by exploiting the relationship noted in equation (4).

$$\hbar\omega = \hbar\frac{8\pi^2}{3\sqrt{3\pi}}\frac{\hbar a_o N_e}{m_e}\sqrt{\frac{E_H}{T_e}}\left[\sum_{i'}\frac{3E_H}{\Delta E_{ii'}}\frac{w_i f_{ii'}}{w_i}g\left(\frac{E}{\Delta E_{ii'}}\right)+\sum_{f'}\frac{3E_H}{\Delta E_{ff'}}\frac{w_f f_{ff'}}{w_f}g\left(\frac{E}{\Delta E_{ff'}}\right)\right]. \quad (5)$$

The Gaunt factor utilized in equation (5) is for the current work the same as the original publications [11, 15], which utilized a table of values with simple analytical corrections for Δn = 0 transitions calculated based on the early Gaunt factors derived in [13]. Above the high temperature limit expressed as $E/\Delta E_{jj'}$ > 50, the Gaunt factor becomes the simple approximation derived in [32] based on the work in [8, 9, 16]. Below $E/\Delta E_{jj'}$< 2 the Gaunt factor becomes 0.2 based again on [9, 13]. This is the method by which the

Dimitrijevic and Konjevic model and the earlier semi-empirical model [9, 11] account for elastic collisions: by extending the calculation to lower energies where inelastic collisions are not energetically available, rather than by calculating them as separate terms as was done in the original semi-classical theory described in [3]. We note that E in this case refers to the average thermal kinetic energy, represented here as $3/2\ T_e$.

While the Dimitrijevic and Konjevic model includes a more complete theoretical treatment than the electron collisional line broadening model originally implemented in ATOMIC, we must recognize it still contains a number of approximations. In order to determine a path forward in eliminating as many of these approximations as practical computational limits will allow we must be able to evaluate potential improvements against the baseline that will be established here. Potential useful improvements include reducing the level of approximation present in the Gaunt factor utilizing additional corrections [33, 34], and improving treatment for heavier ions [35] and for more highly charged ions [36].

Section 3 includes comparisons between measurements of electron collision broadened line widths and theoretical calculations using both the theory originally present in ATOMIC and the Dimitrijevic and Konjevic inspired approach. The atomic structure data input into ATOMIC is calculated utilizing fine-structure calculations that include configuration interaction, and with energy levels adjusted to NIST tabulated values where available [17, 31, 37]. In the first sub-section, we compare select squared radial matrix elements calculated from our fine-structure oscillator strengths to calculations from NIST tabulated oscillator strengths [37].

3. Validation against Published Stark Widths

A series of publications [24-30] initiated at NIST and later conducted in collaboration with other groups has gathered and evaluated measured Stark broadened line widths. The first such publication that we have located is from 1976, and the latest 2009. The rating system assigned is shown in table 1. From 2002 onwards [29, 30], the uncertainty referred to is the relative uncertainty expressed as the root of the sum of the squares of all contributing uncertainties: i.e., parameter uncertainties from T_e, N_e measurements as well as from the measurement of the Stark broadened width ω itself. Prior to 2002 [24-28] the relative uncertainty in these reviews is simply the sum of all contributing uncertainties, and the B+ and C+ ratings implied preference rather than a specific value. In the oldest reviews from the 1970s [24, 25], it is frequently the case that the authors neglected to estimate uncertainty for all parameters, in which case the reviewers estimated the uncertainty based on the authors description. In all critical review papers, the D rating is used only for important transitions for which no other measurement is available, and the relative uncertainty is at least within a factor of 3. For the most recent publication [30] some authors have done their own calculation of relative uncertainty in greater detail than the rating system. In these cases, the number itself has been quoted.

Table 1. NIST Stark Width Rating System

Rating	Uncertainty
A	< 15%
B+	< 23%
B	< 30%
C+	< 40%
C	< 50%
D	> 50%

While we have been guided by the rating system above in selecting experimental data to compare to, we have additional constraints in selecting transitions. Because the model we are evaluating includes

only electron collisional line broadening and these critical review papers evaluate Stark broadening as a whole, we must take care to select papers in which ion broadening is likely to be minimal. Likewise, for lines from neutral elements we must be careful that other sources such as van der Waals broadening were either minimal or measured separately. We emphasize that ATOMIC does include van der Waals broadening for neutrals, but as a separate component from the electron collisional line broadening width being tested here. Likewise, in some experiments optical depth is a concern. If the experimental data suggests doubt about whether a given line is optically thin, and our modeling with ATOMIC suggests it may not be, we again exclude that line from comparison. To avoid as much as possible hydrodynamic instability leading to non-uniform plasma conditions, we have avoided using Stark widths measured in laser-produced plasmas as much as possible. The most stable experiment type discussed in the review articles are long lasting and slowly evolving arc type plasmas, although many other experiment types also exist [24-30]. We utilize only line widths from the spectral range 2500 – 8400Å as the region of greatest applicability for our use in modeling LIBS (laser induced breakdown spectroscopy) experimental data.

For our comparison to data we have selected Ca, O, Fe, and Sn. Calcium is geologically interesting and was featured in the Gaunt factor derivation work of Seaton and Van Regemorter [13, 16]. Oxygen and iron are relevant for astrophysics, industry, and geology. Tin is a semi-metal, defined as a material with a narrow gap between the bottom of the conduction band and the top of the valence band, with high dielectric susceptibility. As such it is useful industrially both for semi-conductor research and EUV lithography.

3.1 Evaluation of Calculated Matrix Elements

Before we compare our calculated Stark broadened line widths to the NIST rated values, it is important to evaluate the accuracy of our radial matric elements. In section 2 we related the square of the radial matrix element to oscillator strengths, which we calculate using the Los Alamos suite of atomic structure codes. The code CATS [31] that produces these oscillator strengths is available online at *http://aphysics2.lanl.gov/tempweb*. Additionally, some rated and measured oscillator strengths are available through the NIST atomic spectral database [37]. We can use these to calculate squared radial matrix elements to compare to examples from our model.

While it is possible to obtain individual squared radial matrix elements from NIST rated experimental oscillator strengths, repeating the full Stark broadened line width calculation would additionally require the oscillator strengths from all scattering channels interacting with the initial and final states of the transition of interest. For example, in a $2p^6 3s - 2p^6 3p$ transition one would need for the initial manifold all other $2p^6 3s$-$2p^6 np$ or $2p^5 n'p$ transitions for the manifold of the initial state, and all $2p^6 ms$-$2p^6 3p$, $2p^6 md$-$2p^6 3p$ and $2p^5 m's$-$2p^6 3p$ transitions for the manifold of the final state. This is not necessarily even exhaustive, since transitions ending in the initial state or beginning in the final state are also included. Even with a practical cutoff of the minimum value of the oscillator strength or the highest *m, n* to consider, it actually requires many more oscillator strengths than just the transition of interest to fill the sum of matrix elements required to determine the Stark broadened line width. For most elements, including those we study here, most of the necessary transitions for our initial and final state manifolds do not have NIST tabulated oscillator strengths. This is one of the primary reasons for the existence of atomic structure models; it is untenable to require the measurement and uncertainty of every transition of every element. Such measurements are, however, indispensible for evaluating the accuracy of atomic structure models, as we will be doing in this section.

Since we cannot repeat the calculation of the D.K.-inspired model using NIST-rated oscillator strengths, we will compare squared radial matrix elements of the transition of interest alone. In the tables below, we will show $R^2_{jj'}$ determined using equation (4) for NIST-rated oscillator strengths (labeled 'NIST'), along with their rating as explained in table 1, to $R^2_{jj'}$ determined from CATS fine-structure (labeled FS) oscillator strengths. We will also include the average percent difference between the NIST and CATS squared radial matrix elements. For tin, we base the uncertainty only on Sn I, since no Sn II oscillator strengths for these transitions are available from NIST.

Table 2. R^2_{ij}, of select Ca transitions

λ[Å]	Transition	NIST R^2_{jj},	Rating	FS R^2_{jj},
4318.7	Ca I $4p^2\ ^3P^o_2 - 4s4p\ ^3P_1$	1.7061	C+	2.4959
3933.7	Ca II $4p\ ^2P^o_{3/2} - 4s\ ^2S_{1/2}$	8.8318	C	10.038
3968.5	Ca II $4p\ ^2P^o_{1/2} - 4s\ ^2S_{1/2}$	4.3113	C	5.0196
		Average % uncertainty:		25.3

Table 3. R^2_{ij}, of select O transitions

λ[Å]	Transition	NIST R^2_{jj},	Rating	FS R^2_{jj},
4368.19	O I $2p^3 4p\ ^3P_0 - 2p^3 3s\ ^3S^o_1$	0.01037	B	0.01326
4368.24	O I $2p^3 4p\ ^3P_2 - 2p^3 3s\ ^3S^o_1$	0.05206	B	0.06685
4368.25	O I $2p^3 4p\ ^3P_1 - 2p^3 3s\ ^3S^o_1$	0.03121	B	0.03988
2733.28	O II $2p^2 4s\ ^2P_{3/2} - 2p^2 3p\ ^2S^o_{1/2}$	1.1968	C	0.9544
3289.98	O II $2p^2 4s\ ^4P_{3/2} - 2p^2 3p\ ^4P^o_{3/2}$	----------	-----	1.0513
4414.91	O II $2p^2 3p\ ^2D^o_{3/2} - 2p^2 3s\ ^2P_{1/2}$	5.3922	B	6.8167
4705.35	O II $2p^2 3d\ ^2F_{7/2} - 2p^2 3p\ ^2D^o_{5/2}$	7.7452	B	7.6259
4860.97	O II $2p^2 3d\ ^2D_{3/2} - 2p^2 3p\ ^2P^o_{1/2}$	5.3289	C	7.3168
		Average % uncertainty:		24.2

Table 4. R^2_{ij}, of select Sn transitions

λ[Å]	Transition	NIST R^2_{jj},	Rating	FS R^2_{jj},
2661.24	Sn I $5p6s\ ^1P^o_1 - 5p^2\ ^3P_1$	0.1051	-----	0.1487
2706.50	Sn I $5p6s\ ^3P^o_2 - 5p^2\ ^3P_1$	1.0692	-----	1.3061
2839.98	Sn I $5p6s\ ^3P^o_2 - 5p^2\ ^3P_2$	1.9634	-----	2.0753
2863.30	Sn I $5p6s\ ^3P^o_1 - 5p^2\ ^3P_0$	1.8852	-----	2.5001
3034.12	Sn I $5p6s\ ^3P^o_0 - 5p^2\ ^3P_1$	0.9189	-----	0.9728
3801.01	Sn I $5p6s\ ^3P^o_1 - 5p^2\ ^1D_2$	0.4505	-----	0.3816
5631.68	Sn I $5p6s\ ^3P^o_1 - 5p^2\ ^1S_0$	0.6304	-----	0.3563
		Average % uncertainty:		23.8

In tables 2-4 we see that for the fine-structure calculation, the average uncertainty is between 23-25% for all elements except iron, for which the uncertainty is significantly larger due to the high level of complexity of the level structure and configuration interaction for this element.

In the following sub-sections, we will also compare to Stark broadened line widths determined from configuration-averaged squared radial matrix elements. We expect this to be a reasonable approximation because each line width includes a sum of many transitions, and the configuration-averaged squared radial matrix element is approximately the sum of all the fine-structure matrix elements that are included in those configurations. For example, in Ca II in table 2, the fine-structure R^2_{jj}, for the 3933.7 and 3968.5 Å lines are the only transitions between those configurations. The configuration-averaged R^2_{jj}, is 15.058, which is very nearly the sum of the two contributing fine-structure transitions in table 2. For a single line, single element calculations such as those shown in the following sections, utilizing fine-structure R^2_{jj}, is an appropriate choice. However, in a real world plasma modeling calculation we will be faced with a multi-element spectrum including thousands of lines or more, and in that environment locating and summing all fine-structure R^2_{jj}, becomes prohibitively slow. We choose to make some approximation in order to be able to do (LIBS) plasma modeling in a realistic amount of time. Given the relationship between configuration-averaged squared radial matrix elements and fine-structure,

and the extensive savings in computational time gained by using configuration-averaged squared radial matrix elements, we expect this to be a reasonable compromise. However, we will include Stark broadened line widths from both fine-structure and configuration-averaged approaches in the following sections so that the potential loss in accuracy may be evaluated. We note that there are two effects that may cause a configuration-averaged matrix element to be different from the sum of included fine-structure matrix elements. If the configuration includes fine-structure levels that do not transition to the level of interest, we would expect the configuration-averaged width to be larger than the total fine-structure width by a corresponding amount. Alternatively, if the fine-structure width includes contributions from configuration interaction, the fine-structure width could be either larger or smaller than the configuration-averaged width, which would not include these effects.

The following sub-sections contain tables summarizing our comparison between measured Stark broadened widths and our theory. Because ATOMIC uses HWHM in eV and measured widths quoted in the critical review publication are either FWHM or HWHM in Å, we select the convention that w refers to the FWHM of a Stark broadened line. We use equation (6) below for this conversion:

$$w[\text{Å}] = 2\hbar\omega[eV]\frac{\lambda^2[\text{Å}^2]}{hc[eV\text{Å}]}. \quad (6)$$

Each table will include the row number to facilitate notes and discussion, the wavelength λ Å of the line, electron temperature T_e in eV and electron number density N_e in cm^{-3}. The widths quoted are w_m for the experimental measurement, w_{cfg} and w_{fs} for the Dimitrijevic and Konjevic-inspired model using configuration-averaged and fine-structure oscillator strengths respectively, and w_H for the old model based on a hydrogenic approximation. We include ratios of the measured width to the width from each theory, as is common in the literature. Below each table we will use notes to list the references for each measured Stark broadened width, the type of experiment and plasma conditions T_e in eV and N_e in cm^{-3}, and the rating given in the review publication. If the rating is a line-specific value based on the experimenter's own determination, we will indicate that and give a range for those values. We note also that we take the measured value from the review publication rather than the original paper in all cases, because the units in these papers have some variation. If a width from either model is within the experimental uncertainty as determined from the rating system in table 1, we show that model width in bold font in the table. Additionally, for tables including more than one comparison, we will show the average of the ratio columns to approximate the aggregate behavior for the ion or neutral species in question.

3.2 Calcium

Table 5. Comparison to measured electron collisional line widths for Ca I

Row	λ[Å]	w_m[Å]	w_{fs}[Å]	w_{cfg}[Å]	w_H[Å]	w_m/w_{fs}	w_m/w_{cfg}	w_m/w_H
1[a]	4318.7	0.155	1.047	0.822	7.272	0.148	0.189	0.019

[a][24, 38] high pressure arc, D rating, T_e = 0.86eV, $N_e = 1.0\text{x}10^{17}cm^{-3}$
For T_e, note that 1 eV is 11604 K.

Only the first review publication treating neutrals rates Ca I measurements. For table 5 we have selected the more accurate of the two experiments, and from that, only the line which the reviewers (and the authors themselves) had the most confidence in, which is the 4318.7 Å [38]. The experiment involved a C cathode used to start the arc, and a Ca anode in an Ar atmosphere [38]. Van der Waals broadening is significant, but also measured separately, while ion collisional broadening is likely to be minimal [38]. The Ar I line 4158.6 Å and ratios of Ca I and Ca II lines are utilized to determine T_e conditions. However, N_e is not determined independently, and the measured Stark broadened line width is instead scaled to N_e =

$1.0x10^{17}cm^{-3}$ [24, 38]. This and the fact that the widths of the Ca II lines from this paper were not accurate enough to be considered for the review, and yet were used in the T_e measurement, are the reasons why this experiment was given a D rating [24]. The D.K.-inspired model is 10 times closer to measurement than the previous hydrogenic model for both fine-structure and configuration-averaged approaches. While this line is sufficiently separate from other members of the multiplet that we don't expect other widths to contribute, the large uncertainty in plasma conditions means it is not clear whether our modeling, done under these conditions, accurately reflects the experiment. We note that, as expected, the difference between the D.K.-inspired model using fine-structure and configuration-averaged approaches is minimal.

Table 6. Comparison to measured electron collisional line widths for Ca II

Row	$\boldsymbol{\lambda}$[Å]	$\mathbf{w_m}$[Å]	$\mathbf{w_{fs}}$[Å]	$\mathbf{w_{cfg}}$[Å]	$\mathbf{w_H}$[Å]	w_m/w_{fs}	w_m/w_{cfg}	w_m/w_H
1[a]	3933.7	0.091	0.188	0.189	2.601	0.483	0.482	0.035
2[b]	3933.7	0.180	0.298	0.299	4.110	0.605	0.603	0.044
3[a]	3968.5	0.085	0.192	0.192	2.648	0.443	0.442	0.032
4[b]	3968.5	0.161	0.303	0.304	4.183	0.532	0.530	0.038
					Average:	**0.516**	**0.514**	**0.037**

[a][28, 39], wall stabilized arc, B+ rating, T_e = 1.054eV, $N_e = 0.8x10^{17}cm^{-3}$
[b][28, 39], wall stabilized arc, B+ rating, T_e = 1.150eV, $N_e = 1.32x10^{17}cm^{-3}$

In table 6 we report results from a more recent experiment with improved accuracy for Ca II involving the 3933.7 and 3968.5 Å doublet [39]. The experimental set up is described in an earlier paper [40] involving Mg. A wall-stabilized arc is generated from water-cooled copper plates. Ca is heated in a furnace, and Ar-H gas is used to lift Ca vapor from the furnace into the center of the arc where the Ca is ionized to Ca II. Reverse flows of Ar-H are used to confine Ca II to the center of the column and keep it away from the end points [39, 40]. Measuring the intensity of Ar I and II lines edge-on determines the T_e value, while N_e is determined from the Stark width of the Balmer H_β from the H impurity [28, 39]. The D.K.-inspired model exceeds measurement by 10% less for the rows at higher temperatures, 2 and 4, than the same lines at lower temperatures in rows 1 and 3. While these models are close to a factor of 2 above measurement, the expected average accuracy in the matrix elements from table 2 is 25%. Since this doublet is not strongly influenced by configuration interaction (the fine-structure and configuration-averaged approaches produce equivalent results within 0.3% here) and the experimental conditions are known within 23% for a B+ rating as indicated in table 1, we would expect the remaining inaccuracy would be due to the gaunt factor in the D.K.-inspired model. This is supported by the apparent temperature dependence of the accuracy, as gaunt factors below threshold for ions lose their temperature sensitivity, and this condition is more easily reached at lower temperatures. The average ratio between the measurement and hydrogenic model is 93% worse than the ratio for the D.K.-inspired model, corresponding to an overestimate of the data greater than a factor of 20.

3.3 Oxygen

In table 7 we examine O I lines from two high accuracy (B+ and A) experiments [41, 42], which were both wall-stabilized arcs. The working gasses were complex mixtures including Ar, He, and H, as well as C in [41] from CO_2. We note C is referenced in [42] as well, but this was from a separate experiment seeking to measure Stark broadened line widths of C lines, not from the same plasma in which the O was measured. In both [41] and [42] plasma density was determined from the Balmer H_β Stark width, while plasma temperature was determined from the plasma composition (identification of lines from elements in the plasma) as well as in [42] relative intensities of O I lines.

The lines studied in [41, 42] include 4368.2 Å and 3947 Å, 5330 Å, and 5436 Å, but we exclude the latter three multiplets due to experimental difficulties in [41, 42]. The 3947 Å line suffered from some

asymmetry in the measurement which reduced the reliability of the experimenter's convolution procedure [41]. 5330 Å and 5436 Å were blended with 'undetermined' additional lines that contributed to the width in [41]. We identify these lines and potential sources of the 'undetermined' blending utilizing [37] and LANL atomic structure data. The 5330 Å line is an unresolved multiplet from $2s^2 2p^3 5d\ ^5D^o_J - 2s^2 2p^3 3p\ ^5P_3$, which is blended with the multiplets at 5329 Å from the levels $^5D^o_J$-$^5P_{1,2}$ of the same $2p^3 5d$-$2p^3 3p$ transition, resulting in a manifold of 9 lines which the experimenters treated as 5330 Å; however, there is also a nearby O II line which may have contributed to the measured width [28, 41]. No additional O I multiplets blend with the transitions $2s^2 2p^3 6s\ ^5S^o_2 - 2s^2 2p^3 3p\ ^5P_J$ centered at 5436 Å; however, this line is bracketed by O II transitions which are possible candidates for the blending observed in the 5436 Å multiplet.

In table 7 we show results from the 4368.2 Å multiplet. Because these three lines are recorded as a blended feature, we determine from our models the net FWHM resulting from the overlap of the three lines that would have been measured in [41,42] by calculating an oscillator strength weighted average of the widths. In this case the D.K.-inspired model is again a little larger than a factor of two more than measurement, and the fine-structure widths are larger than the configuration-averaged widths. The average agreement with data for the configuration-averaged model is 80% better than the hydrogenic model, corresponding to an overestimate of the data by 89%, or a factor of 9. The configuration-averaged model is 20% better than the fine-structure model in this case. We do not believe the configuration-averaged squared radial matrix elements are actually better, so much that the neutral gaunt factor is likely too large, and this somewhat makes up for the underestimate provided by the configuration-averaged approach. This is supported by the variation in accuracy across rows; given that the matrix elements are not dependent on T_e, N_e, this variation is likely due to the neutral gaunt factor.

Table 7. Comparison to measured electron collisional line widths for O I

Row	$\boldsymbol{\lambda}$[Å]	w_m[Å]	w_{fs}[Å]	w_{cfg}[Å]	w_H[Å]	w_m/w_{fs}	w_m/w_{cfg}	w_m/w_H
1[a]	4368	0.780	1.846	1.487	7.156	0.423	0.525	0.109
2[b]	4368	1.440	3.709	3.001	13.65	0.388	0.480	0.105
3[c]	4368.2	0.510	1.092	0.875	4.542	0.467	0.583	0.112
4[d]	4368.2	0.670	1.432	1.150	5.800	0.468	0.583	0.115
					Average:	**0.437**	**0.543**	**0.110**

[a][28, 41] wall-stabilized arc, B+ rating, $T_e = 0.998$eV, $N_e = 0.397 \times 10^{17}$cm^{-3}
[b][28, 41] wall-stabilized arc, B+ rating, $T_e = 1.077$eV, $N_e = 0.784 \times 10^{17}$cm^{-3}
[c][29, 42] wall-stabilized arc, A rating, $T_e = 0.913$eV, $N_e = 0.24 \times 10^{17}$cm^{-3}
[d][29, 42] wall-stabilized arc, A rating, $T_e = 0.946$eV, $N_e = 0.312 \times 10^{17}$cm^{-3}

For O II we present a longer list of lines in table 8 from a series of low power arc experiments. In [43] the arc is generated in a quartz discharge tube with Al electrodes. The working gas is He, which is used to determine plasma N_e through the width of the He II 4686 Å line as described in [29, 44] and the temperature from N II lines present in other experiments discussed in the same work on the same system [43]. Lines at higher T_e and N_e are obtained by reducing the inter-electrode distance in the discharge tube [45, 46]. The working gas was 9:1 O_2 and N_2. T_e was determined using O II to O III line intensity ratios and O II relative intensities [29, 46]. N_e was determined using transmission of a He-Ne laser on axis for laser interferometry at 6328 Å [29,46].

Of the nine O II lines included in table 8, 2733.3 [46], 4414.9 [43], and 4860.9 Å [45] are members of doublets, while 3289.9 [45] and 4705.5 Å [43] are from more complex multiplets. However, unlike 4368 Å [41, 42] in table 4 the separation between these lines and their neighbors is around 1.5-5 Å, while the measured Stark broadened line widths are measured in tenths of Å. We therefore expect all these lines to be experimentally resolved. The D.K. inspired model is within experimental accuracy for both fine-structure and configuration-averaged approaches for rows 3-9 and for row 2 with the

configuration-averaged approach only. For row 1 the D.K.-inspired model produces widths around half the measured value. The Stark broadened line widths from the hydrogenic model exceed measurement by 2 to 5 times. The configuration-averaged and fine-structure approaches have a maximum difference of 26% for rows 1 and 2 and 28% for row 9, but for all other rows agree within 3%. The configuration-averaged and fine-structure models agree with each other within 2.5% on average. However, the hydrogenic model exceeds the data by 76%, corresponding to a factor of 4.

Table 8. Comparison to measured electron collisional line widths for O II

Row	λ[Å]	w_m[Å]	w_{fs}[Å]	w_{cfg}[Å]	w_H[Å]	w_m/w_{fs}	w_m/w_{cfg}	w_m/w_H
1[a]	2733.3	0.648	0.305	0.386	1.404	2.124	1.681	0.462
2[b]	3289.9	0.344	0.277	**0.350**	1.035	1.243	0.984	0.332
3[c]	4414.9	0.087	**0.075**	**0.075**	0.544	1.161	1.168	0.160
4[d]	4414.9	0.113	**0.098**	**0.098**	0.713	1.149	1.157	0.158
5[e]	4414.9	0.135	**0.111**	**0.110**	0.801	1.222	1.230	0.169
6[c]	4705.4	0.115	**0.120**	**0.115**	0.660	0.959	0.999	0.174
7[d]	4705.4	0.170	**0.157**	**0.151**	0.866	1.080	1.125	0.196
8[e]	4705.4	0.189	**0.177**	**0.170**	0.972	1.067	1.114	0.194
9[b]	4860.9	0.284	**0.300**	**0.233**	1.029	0.947	1.219	0.275
					Average:	**1.217**	**1.186**	**0.236**

[a][28, 46] low pressure pulsed arc, B rating, $T_e = 3.447$eV, $N_e = 1.3\text{x}10^{17}\text{cm}^{-3}$
[b][29, 45] low pressure pulsed arc, B+ rating, $T_e = 5.171$eV, $N_e = 0.81\text{x}10^{17}\text{cm}^{-3}$
[c][29, 43] low pressure pulsed arc, B+ rating, $T_e = 1.620$eV, $N_e = 0.31\text{x}10^{17}\text{cm}^{-3}$
[d][29, 43] low pressure pulsed arc, B+ rating, $T_e = 1.646$eV, $N_e = 0.41\text{x}10^{17}\text{cm}^{-3}$
[e][29, 43] low pressure pulsed arc, B+ rating, $T_e = 1.715$eV, $N_e = 0.47\text{x}10^{17}\text{cm}^{-3}$

3.4 Iron

Table 9. Comparison to measured electron collisional line widths for Fe I

Row	λ[Å]	w_m[Å]	w_{fs}[Å]	w_{cfg}[Å]	w_H[Å]	w_m/w_{fs}	w_m/w_{cfg}	w_m/w_H
1[a]	5367.5	1.340	6.093	5.638	28.13	0.220	0.234	0.047
2[b]	5383.3	0.136	0.385	0.400	1.923	0.354	0.341	0.070
					Average:	**0.287**	**0.288**	**0.059**

[a][29, 47] shock tube, A rating, $T_e = 0.776$eV, $N_e = 1.0\text{x}10^{17}\text{cm}^{-3}$
[b][26, 48] Z pinch, A rating, $T_e = 0.816$eV, $N_e = 0.07\text{x}10^{17}\text{cm}^{-3}$

The Fe I lines 5367.5 Å and 5383.3 Å in table 9 are produced by transitions in the $3d^7 4d$-$3d^7 4p$ multiplet. Specifically, 5367.5 Å is the $^5H_4$-$^5G^o_3$ and 5383.3 Å is $^5H_6$-$^5G^o_5$. The D.K.-inspired model is 4-5 times measurement for the 5467.5 Å line, and the configuration-averaged approach is the closer of the two, while the hydrogenic model exceeds measurement by more than 20 times. For the 5383.3 Å line the D.K.-inspired model is within 3 times larger than the measurement, while the hydrogenic model is 15 times larger. The ratios between measurement and model for the configuration-averaged and fine-structure approaches are within 4% for row 2 and 6% for row 1. On average, the D.K.-inspired models differ from the data by 70%, between a factor of 3 and 4, while the hydrogenic model overestimates the data by 94%, or a factor of 19.

While the D.K.-inspired model does represent a significant improvement over the hydrogenic model, we have seen the D.K.-inspired model achieve much closer agreement with measurement for O and Ca. In this instance the disagreement is not caused by potentially inaccurate experimental plasma parameters, as for Ca I, or overlap with other spectral lines, as for O I, but the effects of configuration-interaction. In transition metals like Fe the effects of configuration interaction can result in large numbers of blended

levels for which identifying the jumping electron can be difficult. Due to the sheer number of these levels, we observe an approximately 20% increase in computational time for the new model relative to the hydrogenic. While the D.K.-inspired model is more physically accurate in this regime than the hydrogenic model, and does confer a benefit, it is not accurate enough to achieve agreement with precise measurements for spectra in which the effects of configuration-interaction play a strong role.

3.5 Tin

For tin we rely only on [49]. The measurements were done in a low pressure pulsed arc with He (with a 3% O and 7% N impurity) as a working gas [49]. Similar to [46], laser interferometry is used to determine N_e, and the T_e is determined by the relative ratio between Sn I and Sn II lines from the same electron transitions and for O II to O III line ratios. We note that in [49] the potential influence of resonance and van der Waals broadening is neglected. We note that according to [30] no published theoretical values exist for comparison with [49].

All Sn I lines observed in table 10 are from different fine-structure multiplets of the $5s^25p6s - 5s^25p^2$ transition. The distance between the selected lines and their spectral neighbors significantly exceeds the measured Stark broadened line width, so there are no concerns of blending with other features.

Table 10. Comparison to measured electron collisional line widths for Sn I

Row	λ[Å]	w_m[Å]	w_{fs}[Å]	w_{cfg}[Å]	w_H[Å]	w_m/w_{fs}	w_m/w_{cfg}	w_m/w_H
1[a]	2661.2	0.134	0.242	**0.112**	4.285	0.554	1.197	0.031
2[a]	2706.5	0.164	0.199	0.116	4.321	0.822	1.416	0.037
3[b]	2839.9	0.176	**0.186**	0.109	4.111	0.948	1.621	0.043
4[b]	2863.3	0.124	0.195	**0.111**	4.179	0.637	1.117	0.030
5[b]	3034.1	0.200	**0.182**	0.125	4.692	1.094	1.605	0.043
6[b]	3801.0	0.228	0.359	**0.196**	7.364	0.635	1.166	0.031
7[b]	5361.7	0.424	0.806	**0.429**	16.17	0.526	0.988	0.026
					Average:	**0.743**	**1.301**	**0.034**

[a][30, 49] low pressure pulsed arc, author determined (A to B+), T_e = 1.10eV, $N_e = 0.60 \times 10^{17}$cm^{-3}
[b][30, 49] low pressure pulsed arc, author determined (A to B+), T_e = 1.12eV, $N_e = 0.51 \times 10^{17}$cm^{-3}

Because these lines are from the same configuration, differences in the configuration-averaged widths are due to the transition wavelength (which is very similar between rows 1 and 5 but changes more sharply between row 6 and row 7) and the T_e, N_e conditions, which are equivalent for all rows but the first two. Some of the D.K.-inspired model results for fine-structure or configuration-averaged approaches agree with experiment within 16%, which is the experimental uncertainty for these lines. For other results such as the fine-structure in row 1 or the configuration-averaged in row 3 the alternative model is within a factor of two larger or smaller, where the fine-structure approach tends to exceed measurement and the configuration-averaged approach tends to be smaller than measurement. For row 2 the fine-structure approach is within 28%, while the configuration-averaged approach is within 40% of measurement. We note that for the Sn I lines in table 11 configuration interaction effects are very significant, and as such the width obtained using fine-structure can be up to a factor of two larger than the configuration-averaged approach, such as in rows 1, 6, and 7. The average ratio between the measurement and the D.K.-inspired model results in agreement within 26% for the fine-structure approach or 30% for the configuration-averaged approach, where the fine-structure typically overestimates the measurement, and the configuration-averaged approach is an underestimate. The hydrogenic model exceeds the data by 97% on average, which is close to a factor of 30.

For Sn II in table 11 we again use the results of [49]. While additional experimental data is available from [50, 51], these measurements do not obey the same T_e, N_e trends as [49] and were given C and D ratings in the reviews. We therefore elect to exclude these additional data. For Sn II we note the

term description for these transitions are not listed in the NIST atomic spectral database for this spectral range [37], only the wavelengths and some levels. We have relied on our calculated atomic structure data from CATS [31] and the term description from [30, 49] to identify each line.

Table 11. Comparison to measured electron collisional line widths for Sn II

Row	λ[Å]	w_m[Å]	w_{fs}[Å]	w_{cfg}[Å]	w_H[Å]	w_m/w_{fs}	w_m/w_{cfg}	w_m/w_H
1[a]	3472.5	0.496	2.977	2.542	10.97	0.167	0.195	0.045
2[a]	3841.4	0.660	1.849	2.196	16.35	0.357	0.301	0.040
3[a]	5332.4	0.298	3.551	1.915	14.97	0.084	0.156	0.020
4[a]	5562.0	0.355	2.569	2.083	16.28	0.138	0.170	0.022
5[a]	5588.9	0.310	2.125	1.221	6.203	0.146	0.254	0.050
6[a]	5797.2	0.548	1.669	1.313	6.673	0.328	0.417	0.082
7[a]	5799.2	0.366	1.647	1.314	6.677	0.222	0.279	0.055
8[a]	6453.5	0.428	1.738	0.982	15.47	0.246	0.436	0.028
9[a]	6844.1	0.560	3.793	1.014	17.39	0.148	0.507	0.032
					Average:	**0.204**	**0.302**	**0.042**

[a][30, 49] low pressure pulsed arc, author determined (A to B+), T_e = 1.12eV, N_e = 0.51x10^{17}cm^{-3}

Line 3472.5 Å is $5s^2 7d\ ^2D_{3/2}$-$5s^2 6p\ ^2P^o_{1/2}$, and 3841.4 Å is $5s^2 8s\ ^2S_{1/2}$-$5s^2 6p\ ^2P^o_{3/2}$. These are the only included lines from these transitions. Lines 5532.4 and 5562.0 Å are produced by the multiplet $5s^2 6d\ ^2D_{3/2,5/2}$-$5s^2 6p\ ^2P^o_{1/2,3/2}$, the third member of which resides at 5597 Å but was not measured. The lines in rows 5-7 are produced by the $5s^2 4f\ ^2F^o_{5/2,\ 7/2}$-$5s^2 5d\ ^2D_{3/2,\ 5/2}$ multiplet. These lines are sufficiently separated from each other and any neighboring lines that spectral overlap is not a concern. The 6453.5 and 6844.1 Å lines are a doublet produced by $5s^2 6p\ ^2P^o_{1/2,3/2}$-$5s^2 6s\ ^2S_{1/2}$. They have been frequently measured historically because they are very distant from each other and in a spectrally sparse region. The D.K.-inspired model is between 3 times larger than measurement in row 2 to 10 times measurement in row 3 in fine-structure, with somewhat smaller widths in the configuration-averaged approach. For rows 6, 8 and 9 the configuration-averaged approach is within a factor of 2-3 of measurement. The hydrogenic model is between 20 and 35 times larger than measurement. On average, the D.K.-inspired model is 10% closer to the data for the configuration-averaged model than the fine-structure approach, where the configuration-averaged result is within 70% of the measurement. The hydrogenic model exceeds measurement by 96%, or a factor of 25.

3. 6 Model Sensitivity to T_e, N_e Parameters

In this subsection we explore the behavior of Stark broadening with respect to plasma parameters, with the goal to obtain a better understanding of ATOMIC's capability to accurately obtain plasma conditions from spectroscopic modeling of experimental plasmas. As we observe in equations (1), (3), and (5) electron collisional line broadening formulas include an $N_e/\sqrt{T_e}$ dependence, while equations (3) and (5) based on the new model include additional temperature dependencies through the Gaunt factor, which differs between ions and neutrals. There are no additional explicit N_e dependencies in the newer models.

In figure 1, we study the T_e and N_e trend for the O II line at 4705.4 Å. While the Stark widths for the hydrogenic model are significantly larger than the experiment, they follow the linear N_e and $1/\sqrt{T_e}$ dependencies explicitly. The new model shows slightly different T_e trends from the experiment, which is an indication that improving the Gaunt factors in these models, the only additional source of T_e dependence, may have significant benefits. The slightly different N_e trend observed in the new model is partially due to the incomplete T_e scaling, which is more difficult than in the N_e-scaled case in Figure 1a) due to the fact that only the leading inverse root of T_e factor may be divided out.

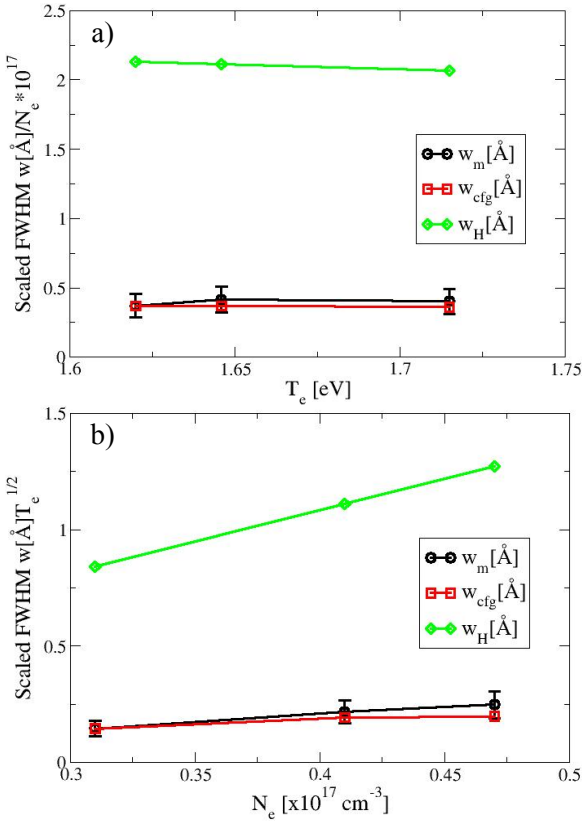

Figure 1. The T_e, N_e dependence of the 4705.4 Å O II line from table 8. In a), all widths are scaled to $N_e = 1.0\text{x}10^{17}$ [cm^{-3}] to isolate the T_e dependence of the line, by dividing the width by $N_e/1\text{x}10^{17}$. In b) all widths are multiplied by $\sqrt{T_e}$ to remove some of the T_e dependence, which is not equivalent to scaling all widths to $T_e = 1.0$eV because the Gaunt factor in the new model also depends on T_e.

In prior subsections we observed that the Stark broadened line widths produced by the hydrogenic model are consistently larger than measurement. One of the reasons for this is that this model excludes Gaunt factors, which in this regime are often significantly smaller than one. As an example, we can refer to table 6 for Ca II. In this instance, while the D.K.-inspired model is closer to experimental data, it does not obey the same T_e, N_e trend as measurement. Conversely, the hydrogenic model is less accurate, but the degree of change between the two sets of plasma conditions is about the same as experiment. This is some additional indication that the degree of T_e dependence introduced by the Gaunt factor in the D.K.-inspired model has some room for improvement.

4. Electron collisional line broadening and LIBS

Our new line broadening method was recently used to model the LIBS spectrum of basalt as discussed in detail in [19]. Here we show for an optically thin region of the basalt spectrum from BIR-1A a comparison to radiation transport calculations done using the same three layer spherical plasma and T_e, N_e, and L values as [19]. The ATOMIC runs input to this model were done using either the hydrogenic model or the D.K.-inspired model using configuration-averaged oscillator strengths. In order to reconcile the intensity units of our radiation transport models with the arbitrary experimental units we have scaled the background level of our calculations to the background of the data. The two radiation transport calculations are scaled together, so the intensity relationship between the two calculations is unchanged, but the pair are scaled to figure 2a and 2b independently because the units of the two spectrometers are

not equivalent. Within this context, we discuss the qualitative agreement between each radiation transport model and the experimental data.

The D.K.-inspired model in figure 2a is much more similar to the experimental intensity of the O I $2p^3 3p\ ^5P_2 - 2p^3 3s\ ^5S^o_2$ transition at 7770 Å than the hydrogenic model, and the line width of the D.K.-inspired model is also very similar to the width of the experiment, while the hydrogenic model is significantly broader.

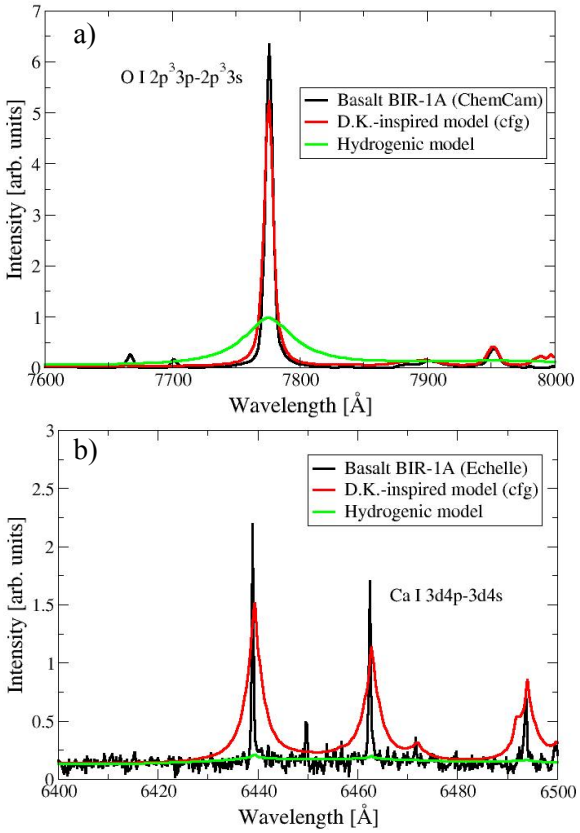

Figure 2. Lines from the radiation transport analysis of the optically thin Near-IR spectral range of the basalt BIR-1A analysis from [19]. ATOMIC has been run utilizing either the hydrogenic Stark broadening model or the D.K.-inspired model. Intensity was determined from each set of emissivities using the radiation transport method of [19]. The basalt data were taken using the same laser and target, but different spectrometers.

Figure 2b includes lines from the Ca I 3d4p-3d4s multiplets identified with the help of the NIST atomic spectral database [37] and CATS atomic structure data [31]. The strong lines at 6439.0 Å and 6462.5 Å are produced by the $^3F^o_4$-$^3D_3$ and $^3F^o_3$-$^3D_2$ transitions, respectively. The line at 6456.0 Å is from the $^1D^o_2$-$^3D_2$ transition, while the lines at 6472, and 6494 Å are produced by other members of the ^3D_J-$^3F^o_J$, multiplet. We note that the amount of broadening imparted by the D.K.-inspired model for the two strong Ca I 3d4p -3d4s lines exceeds the amount of broadening evident in the experiment; however, the previous hydrogenic model so overestimated the Stark broadening for these lines that their intensities are suppressed, so this model would not have been suitable for modeling data from the higher resolution Echelle spectrometer (resolving power 11000 in this spectral range).

The use of the hydrogenic model for Stark broadened line widths would have resulted in considerably different T_e, N_e conditions for the radiation transport analysis than were determined for the basalt BIR-1A spectrum in [19] using the D.K.-inspired model. We can also say based on our comparisons to rated experimental Stark broadened line widths in section 3 that these T_e, N_e conditions would be less accurate than the ones obtained utilizing the D.K.-inspired model. However, because of the

presence of elements heavily influenced by configuration interaction such as Fe and Mn in basalt, the D.K.-inspired model took 40% longer to run than the hydrogenic model for this complex, multi-element spectrum. This was not prohibitively expensive in part because the conditions for all three layers used in the radiation transport analysis fall within the range of the local thermodynamic equilibrium (LTE) approximation, as was verified using ATOMIC in [19]. Unfortunately, because the accuracy of the new model depends on whether a given line is produced by a transition influenced by the effects of configuration-interaction, whether a line is part of a fine-structure multiplet which is resolved or un-resolved, and whether the line overlaps with any other spectral features, it is difficult to determine an overall N_e sensitivity for the plasma model. However, for a simpler plasma containing a single element, such as those used in section 3, the observed trends in line broadening behavior may enable such an estimate in the future.

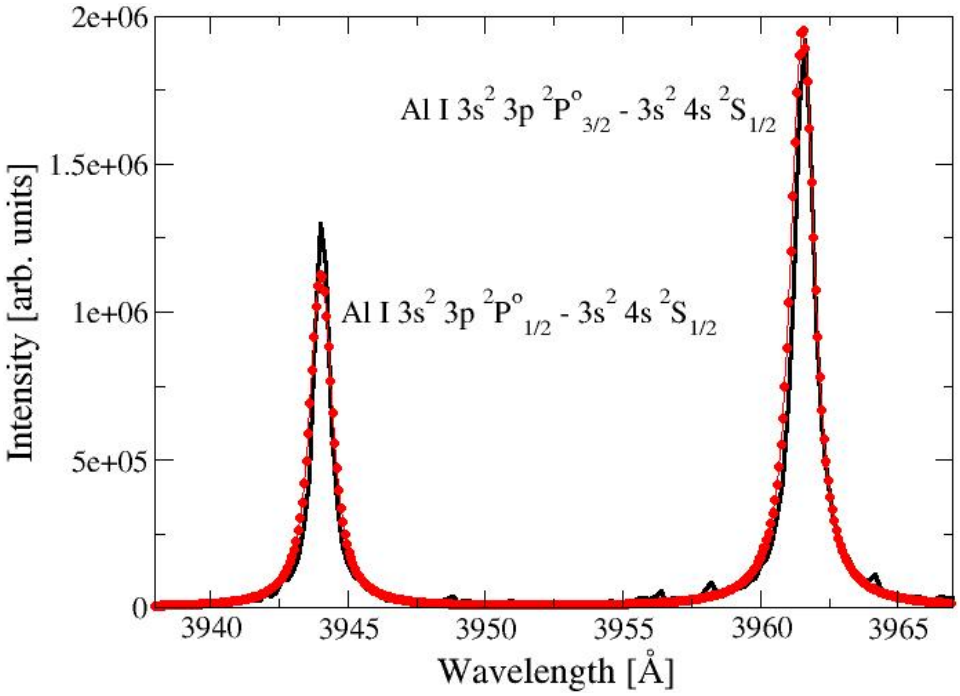

Figure 3: Analysis of two Al I lines from an aluminum alloy plasma using the Dimitrijevic and Konjevic model. We obtain for this model plasma parameters of $T_e = 1.2\pm0.1$eV, $\rho = 6.86\text{x}10^{-6}\pm0.49\text{x}10^{-6}$g/cm^3, $N_e = 1.50\text{x}10^{17}\pm0.11\text{x}10^{17}$cm^{-3} for a sphere of radius $R = 3.0\text{x}10^{-2}\pm0.5\text{x}10^{-2}$ cm. Changes within this range result in changes to intensity visually comparable to small fluctuations observed in the continuum between the two lines of interest. As the data is in arbitrary units, the model solution is scaled to the mean of the continuum between the two lines in the region of 3947-3956 Å. We show the model solution in red with diamonds and the data in black. We note that the wavelength axis of the model has been corrected by -1.131 Å to account for transmission through air [31].

An example of a simpler LIBS plasma model is featured in figure 3. This is from the LIBS spectrum of an aluminum alloy that is 95-98% Al, and containing small percentages of Cr (0.04-0.35), Cu (0.15-0.4), Fe (<0.7), Mg (0.8-1.2), Mn (<0.15), Si (0.4-0.8), Ti (<0.15) and <0.15 total other possible contaminants. While these contaminant elements make up only between 2 and 5% of the mass of the sample, they are spectroscopically active and will have an outsized contribution to the common electron density due to their large numbers of electrons. The experiment was done on the Echelle spectrometer in the lab at Los Alamos using a 54mJ laser pulse with 500ns delay time and 1μs integration time. The data presented represent the net result of 10 shots.

Because these Al I lines are characteristically very strong but may also be strongly absorbed by layers of cooler plasma, reproducing the strength of these lines essentially requires a single layer. This

does not mean that the plasma is uniform, but that the Al I that is responsible for the emission of these lines likely comes from a layer near the outside of the plasma. Higher temperatures quickly result in the loss of these spectral lines in favor of Al II, beginning at 1.4eV, while lower temperatures even for the single onion shell approach result in strong attenuation below 1.0eV. The volume of the region containing Al may be represented by a spherical shell with $R \leq 0.03$cm. The conditions quoted for figure 3 are representative only of the region of the plasma responsible for emitting these lines. If we examine figure 3, we note that the ratio of the two lines is around 1.5:1 in favor of the 3961.5 Å line. Given that like the basalt model this is in LTE, we would expect that if the oscillator strengths of this doublet are equivalent, as shown on the NIST website, (f_{ij} = 0.116) [37], the ratio of the emissivities of the two lines would be 2:1. The oscillator strengths from CATS are very nearly equivalent, at 0.1311 and 0.1306 for the fine-structure and 0.1307 for the configuration-averaged. The expected 2:1 ratio is disturbed in the actual intensity by a small amount of attenuation due to the optical depth of these lines (0.1377 and 0.2627). Since the optical depth of the brighter line is also larger, it is attenuated slightly more as well.

We also note that in the NIST rated publication [28] there is a C rated measurement of the electron collisional line width of the 3944.1 Å and 3961.5 Å lines of w = 0.84 Å at T_e = 1.008eV and $N_e = 2.5\text{x}10^{17}\text{cm}^{-3}$. If we run this calculation through our model at these conditions, we obtain for the 3944.1 Å line 1.535 Å in fine-structure and 1.182 Å in configuration-averaged modes. For the 3965.1 Å line we obtain 1.5206 Å in fine-structure and 1.192 Å in configuration-averaged. The average ratio between the measurement and model for fine-structure is 0.553, while the average ratio in configuration-averaged mode is .708. This means that our configuration-averaged model, which was used to generate figure 3, is likely over-predicting the N_e of this plasma layer by 30%, which is, however, well within the C rating for these lines. We do not expect the temperature is as strongly affected because as previously explained the line intensities are strongly correlated to the plasma temperature.

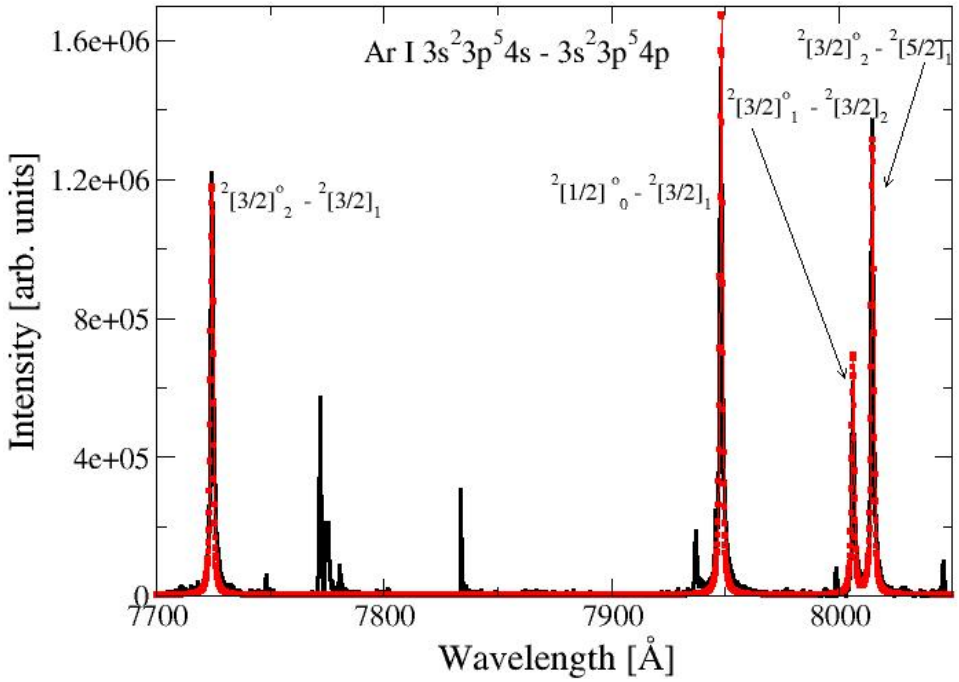

Figure 4. Analysis of four Ar I lines from the $3s^2\ 3p^5 4s - 3s^2 3p^5 4p$ multiplet, where the individual lines are identified as in the NIST atomic spectral database [37] using jK coupling notation. The model fit is shown in red with squares, and the spectrum in black. We obtained plasma conditions of T_e = 1.0eV, $\rho = 0.8\text{x}10^{-5}\text{g/cm}^3$, $N_e = 3.57\text{x}10^{16}\text{cm}^{-3}$ for an optically thin plasma layer R = .01cm. We note these lines were corrected for transmission through air by -1.931 Å [31]

The spectrum shown in figure 4 is from a LIBS measurement of an FeO sample shot at LANL in an atmosphere of 8 torr of Ar. The two groups of lines bracketing 7800 Å are from O. Further analysis of this measurement will be provided in a forthcoming paper. The determined plasma conditions are representative of the average within this spectral window. There are indications that the larger plasma spectrum is from a multi-layer system, in which case the total intensity would be generated by regions whose conditions are approximated by the 1 layer representation here. As such, it is difficult to assign as precise a sensitivity range as determined for figure 3. We note that we have examined conditions between ρ of $0.4x10^{-5}$-$1.6x10^{-5}$g/cm^3 and T_e of 0.6eV to 0.8eV and have not observed the development of appreciable optical depth, so if multiple layers are required to model this system we expect this spectral window will remain optically thin. T_e above 1.2eV and higher densities than we attempted would likely be required to generate appreciable attenuation, which does not appear representative of this plasma at the current stage of analysis. We note changes in T_e by 0.2eV are sufficient to double (or halve) the line intensity, where in this case reducing the temperature results in increased line emission and thinner lines due to reduced broadening and fewer transitions into Ar II. Changes in density by $0.2x10^{-5}$g/cm^3 result in changes to the line width and line intensity of approximately 25% (where a higher ion density results in higher emission due to a larger number of free electrons, but also a thicker line for the same reason).

The 7723.76 Å line in figure 4 has measured and rated Stark broadened line widths [30] at 3 different sets of conditions, T_e = 1.379eV and $N_e = 0.7x10^{17}$cm^{-3}, T_e = 1.344eV, $N_e = 0.67x10^{17}$cm^{-3}, and T_e = 1.396eV and $N_e = 0.71x10^{17}$cm^{-3}. The corresponding widths are 0.844 Å, 0.774 Å, and 0.855 Å with a B+ rating. If we run our model for this line at these conditions, we would obtain for the fine-structure mode widths of: 3.015 Å, 2.871 Å, and 3.0655 Å, and for the configuration-averaged mode used in figure 4 widths of: 1.193 Å, 1.666 Å, 1.787 Å. The average ratio between measurement and model for fine-structure is 0.273, while the average ratio between measurement and configuration-averaged is 0.544. The difference between this average and the previous case is that rather than averaging across multiple lines, this is a single line for multiple T_e, N_e conditions, and the ratio changes between 0.447-0.708 for the three sets of conditions. This implies that the T_e, N_e dependence of the neutral gaunt factor has a large range in accuracy across plasma conditions. If we were in the same plasma regime, therefore, our model would be overestimating N_e by 46%. However, given the fact that the conditions are not equivalent, the average in this case does not appear representative.

5. Conclusions

In this work we have introduced a new effort to improve electron collisional line broadening in the LANL plasma modeling code ATOMIC. Previous computational limitations meant that this code, which is capable of modeling upwards of millions of lines for either single or multi-element plasmas, relied on a hydrogenic approximation for electron collisional line broadening. We improve on this by utilizing a pair of models for neutrals and ions by Dimitrijevic and Konjevic, designed with low temperature plasmas in mind. While these older models are semi-classical and semi-empirical, we have incorporated into our model modern configuration-averaged oscillator strengths calculated by LANL's atomic structure codes. We have compared the results to calculations utilizing fine-structure oscillator strengths and have found that, except for cases in which configuration interaction strongly influences the manifold of scattering channels which broaden a transition, the use of configuration-averaged oscillator strengths leads to widths that are within a few percent of the accuracy of the Stark broadened line widths calculated using fine-structure oscillator strengths. This approximation tends to produce smaller widths than the full fine-structure approach for the transitions tested here. We note that both our fine-structure and configuration-averaged oscillator strengths are computed with CATS, which is available online, and the required equations for determining the electron collision broadened line width are included. Likewise, other sources of oscillator strengths, line strengths, or squared radial matrix elements may be used. Therefore, while we utilize ATOMIC for our plasma modeling, the modifications we have made to the Dimitrijevic

and Konjevic semi-empirical approach are generally applicable to the regime of low temperature near-neutral plasmas.

We have studied the comparison between the hydrogenic model and the D.K.-inspired model for lines from neutrals and singly ionized species in a series of elements including Ca, O, Fe, and Sn. The intent was to develop an understanding of the range of applicability of this model, the level of improvement obtained relative to the prior model, and to determine whether continuing work to improve the approximations in this approach is justified. Our best comparison was obtained with O II and Sn I, for which several of the modeled lines achieved agreement within the uncertainties of the experimental data. For Ca I, II and O I we were on average within a factor of two of experiment. For Sn II for which the level structure is blended due to configuration interaction, the D.K.-inspired model is more like a factor of 3 from the data. It is only for Fe, for which the spectrum is dominated by complex configuration interaction, that the agreement of the D.K.-inspired model exceeds this ratio. Conversely, the hydrogenic model is between 4 and 30 times larger than the D.K.-inspired model, depending on the element. This overestimate is large enough to render the hydrogenic approximation unsuitable for modeling electron collisional line broadening in this plasma regime. If the average ratio between the data and the model is representative, the configuration-averaged approach produces results that are within 10% of the accuracy of the fine-structure approach, however, it tends to be smaller than the fine-structure approach for the elements examined here.

The computational speed of the new model is equivalent to the old, except for elements in which the effects of configuration-interaction play an important role, such as iron, for which run time for the new model is 20% longer than the old hydrogenic approach, per element. Based on these results we find that the new D.K.-inspired approach appears to be a reasonable approximation for spectra that include fine-structure from the *s*- and *p*- subshells (such as O and Sn), with no expected increase in computational run-time, but is both less accurate and more computationally demanding for transitions involving levels with open *d*-subshells and higher (such as Fe and the Ca 3d4p-3d4s transition examined in section 4). However, because the new approach was able to match measured Stark widths within error bars for a limited number of lines, further improvements to increase the accuracy of this model are both justified and advisable.

Based on the T_e dependence observed in subsection 3.5, which differed from the experiment, we can deduce that the Gaunt factors used in the original papers by Dimitrijevic and Konjevic might be improved upon by more accurately accounting for corrections for elastic collisions, path curvature of perturbing electrons interacting with an ion, and polarization effects for neutrals. Additionally, the original D.K. model approximated the velocity average over the perturbing electrons at the root mean square velocity. It is possible to remove this approximation by averaging over the electron's kinetic energy for a broader range of velocities. We intend to pursue this approach in the future.

We have also evaluated the D.K.-inspired model and the hydrogenic model in the context of a real world radiation transport calculation involving LIBS basalt BIR-1A experimental data [19] for select lines, for which the D.K.-inspired model has already been used. The agreement obtained between the resulting spectra and experiment is consistent with the behavior observed from comparison to rated experimental Stark broadened widths. We expect that the improvement in accuracy of the D.K.-inspired model over the hydrogenic model to translate into T_e and N_e values that are closer to actual plasma conditions through some combination of reduced N_e and increased T_e values, relative to the hydrogenic model. We hope to utilize this information to evaluate radiation transport model agreement to experiment more quantitatively in the future. We gave a small example of how this would work utilizing an Al alloy plasma and Ar lines from an FeO plasma in an Ar atmosphere. In this case, we selected interesting lines from the plasma that could be approximated by a single region without significant optical depth, and determined a synthetic spectrum with ATOMIC that was visually in good agreement with the data. We then compared a NIST rated measurement of the Stark broadened line width of one or two of the lines examined to our model prediction at those conditions, and used that result to determine that in these cases our fit with ATOMIC was between 30% of the real plasma conditions for Al. For Ar the situation was more complicated. The average result indicated that we would be within 45% of plasma conditions, but

there was significant variation in accuracy for the three T_e, N_e conditions at which line widths were measured, which is a further indication that improvements in the accuracy of the D.K.-inspired model could be gained by focusing on the T_e, N_e dependence of the gaunt factors for both neutrals and ions.

Acknowledgements
We gratefully thank the researchers at NIST and other institutions who have taken time to critically review the extensive literature on experimentally measured Stark widths. Without these review publications, selecting experimental data of sufficient quality and comparability to our model would have been prohibitively difficult. We hope that these organizations continue to support the community of Stark-broadening theorists and experimentalists by continuing this endeavor into the future.

This work was partially supported by Laboratory Research and Development funding.

The Los Alamos National Laboratory is operated by Los Alamos National Security, LLC for the National Nuclear Security Administration of the U.S. Department of Energy under Contract No. DEAC52-06NA25396.

References

[1] Baranger M 1958 *Physical Review* **111** 481
[2] Baranger M 1958 *Physical Review* **112** 855
[3] Baranger M 1962 *Atomic and Molecular Processes* ed Bates D R Academic Press New York 493
[4] Lorenzen S Omar B Zammit M C Fursa D V Bray I 2014 *Phys. Rev. Exi* **89** 023106
[5] Ralchenko Y V Griem H R Bray I 2003 *Journ. Quant. Spectrosc. Radiat. Transfer* **81** 371
[6] Elabidi H Nassib N B Dimitrijevic M S 2006 *New Astronomy* **12** 64
[7] Sahal-Brechot S Dimitrijevic M S Nessib N B 2014 *Atoms* **2** 225
[8] Griem H Baranger M Kolb A C Oertel G 1962 *Phys. Rev. E* **125** 177
[9] Griem H R 1968 *Phys. Rev. E* **165** 258
[10] Dimitrijevic M S Konjevic N 1978 *Journ. Quant. Spectrosc. Radiat. Transfer* **19** 407
[11] Dimitrijevic M S Konjevic N 1980 *Journ. Quant. Spectrosc. Radiat. Transfer* **24** 451
[12] Seaton M J 1962 *Proc. Phys. Soc.* **79** 1105
[13] Regemorter H V 1962 *Astro. Phys. J.* **36** 906
[14] Dimitrijevic M S Konjevic N 1986 *Astron. Astrophys.* **163** 297
[15] Dimitrijevic M S Konjevic N 1987 *Astron. Astrophys.* **172** 345
[16] Seaton M J 1962 *Atomic and Molecular Processes* ed Bated D R Academic Press New York 493
[17] Colgan J Judge E J Kilcrease D P Barefield J E II 2014 *Spectrochimica Acta Part B* **97** 65
[18] Noll R 2012 *Laser-Induced Breakdown Spectroscopy* Springer-Verlag Heidelberg
[19] Colgan J Judge E J Johns H M Kilcrease D P Barefield J E II McInroy R Hakel P Wiens R C Clegg S M 2015 *Spectrochimica Acta Part B* **110** 20-30
[20] Wiens R C et al 2013 *Spectrochimica Acta Part B* 1-27
[21] Armstrong B H Johnson R R Dewitt H E Brush S G 1966 Opacity of high temperature air ed. Rouse C A *Progress of high temperature physics and chemistry* vol 1 Pergamon Press New York 169
[22] Mancini R C Kilcrease D P Woltz L A Hooper C F 1991 *Computer Physics Communications* **63** 314
[23] Hooper C F 1966 *Physical Review* **149** 77
[24] Konjevic N Roberts J R 1976 *J. Phys. Chem. Ref. Data* **5** 209
[25] Konjevic N Wiese W L 1976 *J. Phys. Chem. Ref. Data* **5** 259
[26] Konjevic N Dimitrijevic M S Wiese W L 1984 *J. Phys. Chem. Ref. Data* **13** 619
[27] Konjevic N Dimitrijevic M S Wiese W L 1984 *J. Phys. Chem. Ref. Data* **13** 649
[28] Konjevic N Wiese W L 1990 *J. Phys. Chem. Ref. Data* **19** 1307
[29] Konjevic N Lesage A Fuhr J R Wiese W L 2002 *J. Phys. Chem. Ref. Data* **31** 819
[30] Lesage A 2009 *New Astronomy Reviews* **52** 471

[31] Cowan R D 1981 *The Theory of Atomic Structure and Spectra* Los Alamos Series in Basic and Applied Sciences University of California Press: Berkeley, California
[32] Griem H R 1974 *Spectral Line Broadening* Academic Press Pure and Applied Physics 39 New York 256
[33] Younger S M Wiese W L 1979 *Journ. Quant. Spectrosc. Radiat. Transfer* **22** 161
[34] Fisher V I Ralchenko Y V Bernshtam V A Goldgirsh A Maron Y Vainshtein L A Bray I Golgen H 1997 *Phys. Rev. A* **55** 329
[35] Dimitrijevic M S Konjevic N 1983 *Journ. Quant. Spectrosc. Radiat. Transfer* **30** 45
[36] Dimitrijevic M S Sahal-Brechot S Bommier V 1991 *Astron. Astrophys. Suppl. Ser.* **89** 581
[37] Kramida A Ralchenko Yu Reader J and NIST ASD Team 2014 *NIST Atomic Spectra Database* v 5.2. Available Online: http://physics.nist.gov/asd 2015, June 1 National Institute of Standards and Technology Gaithersburg MD
[38] Huhn R Kusch H J 1973 *Astron. Astrophys* **28** 159
[39] Goldback C Nollez G Plomdeur P Zimmerman J P 1983 *Phys. Rev A* **28** 234
[40] Goldback C Nollez G Plomdeur P Zimmerman J P 1982 *Phys. Rev A* **25** 2596
[41] Goly A Weniger S 1987 *J. Quant. Spectrosc. Radiat. Transfer* **38** 225
[42] Mijatovic Z Konjevic N Kobilarov R Djurovic S 1995 *Phys. Rev. E* **51** 613
[43] Blagojevic B Popovic M V Konjevic N 1999 *Physica Scripta* **59** 374
[44] Djenize S Sreckovic A Labat J Platisa M 1991 *Z. Phys. D* **21** 295
[45] Djenize S Milosavljevic V Sreckovic A 1998 *Journ. Quant. Spectrosc. Radiat. Transfer* **59** 71
[46] Puric J Djenize S Sreckovic A Platisa M Labat J 1988 *Phys. Rev. A* **37** 498
[47] Lesage A Lebrun J L Richou 1990 *The Astrophysical Journal* **360** 737
[48] Freudenstein S Cooper J 1979 *Astron. Astrophys.* **71** 283
[49] Djenize S Sreckovic A Nikolic Z 2006 *J. Phys. B* **39** 3037
[50] Miller M Roig R A Bengston R D 1979 *Phys. Rev. A* **20** 499
[51] Puric J Cuk M Lakicevic I S 1985 *Phys. Rev. A* **20** 1106